Fibers and Polymers 2017, Vol.18, No.3, 525-532
DOI 10.1007/s12221-017-6710-1

ISSN 1229-9197 (print version)
ISSN 1875-0052 (electronic version)

An Improved Lagrangian Approach for Simulating Fiber Whipping in Slot-Die Melt Blowing

Sheng Xie*, Yongchun Zeng[1], Wanli Han, and Guojun Jiang[2]

College of Material Textile Engineering, Jiaxing University, Jiaxing 314000, P.R. China
[1]*Key Laboratory of Textile Science & Technology, Donghua University, Ministry of Education, Shanghai 201620, P.R. China*
[2]*Zhijiang College of Zhejiang University of Technology, Hangzhou 310024, P.R. China*
(Received July 6, 2016; Revised October 20, 2016; Accepted October 30, 2016)

Abstract: Melt blowing is a one-step approach for manufacturing microfibrous nonwovens. In slot-die melt blowing, a pair of air jets with high velocity and temperature is applied on the polymer and attenuates the polymer in to fibers. The fiber motion which was called vibration or whipping plays a crucial role in expressing the drag mechanism. In this study, an improved Lagrangian numerical approach was utilized to simulate the fiber whipping in melt blowing. The fiber whipping simulated in this study was significantly improved compared to other previous works. Meanwhile, the fiber diameter, fiber velocity and fiber temperature below the spinneret were simulated. The numerical simulation indicated that the most attenuation of fiber diameter occurred within 0.07 m below the spinneret; the fiber velocity increased gradually while the air velocity decreased rapidly along the spinning line, and the fiber velocity exceeded the air velocity where below a critical *z*-position; In addition, the fiber temperature decreased tardier than the decreasing of air temperature. This study illustrated that it was important to optimal design the air flow field which was supposed to fully utilize the air velocity and temperature together. In addition, the energy saving of melt blowing deserved to be taken into consideration.

Keywords: Melt blowing, Fiber whipping, Numerical simulation, Lagrange

Introduction

Melt blowing applies air flow field to attenuate polymer into microfibrous nonwovens. Much works have been done on the air flow field and fiber motion in melt blowing. Shambaugh and his coworkers systematically studied the melt-blowing air flow field via methods of CFD simulation [1-4] and experimental measurements [5-8]. Their work provided the basic characteristics of air flow field in melt blowing.

The fiber motion in melt blowing plays a major role in understanding the attenuation effect between air and polymer (fiber). Similarly, researchers used experimental and theoretical methods to achieve the fiber motion. The fiber vibration was firstly recorded by Shambaugh and his coworkers [9] via the technology of high speed photograph. At that time, they captured a bundle of fibers instead of single fiber, and the bundle of fibers appeared to be splaying. Bresee *et al*. [10-12] also devoted some experimental works to fiber motion. However, their works didn't discover the law of fiber whipping which was majorly due to the air velocities they used were much lower than the industrial levels. Our previous work [13] captured the fiber whipping by high speed camera with the image size of 26.2 mm× 19.6 mm and 64.9 mm×64.9 mm respectively in melt blowing, this work discovered that fiber whipping in the slot-die melt blowing appeared to be a fiber path with two groups of loops moving downward. Refer to the theoretical research on fiber motion, Shambaugh and his coworkers [9,14,15] built 1-dimensional, 2-dimensional and 3-dimensional models successively to predict the fiber diameter in melt blowing. Some theoretical researches also have been done by other researchers [16-20]. Their works had a significant contribution to the research on fiber attenuation in melt blowing. Sun *et al*. [21] built an Euler-Lagrange numerical model to simulate the fiber whipping during melt blowing by regarding the fiber as beads, with their model, some parameters could be tracked during the whole melt blowing. Their work provided an intuitively understanding of the fiber attenuation. However, the lateral amplitude of the fiber whipping simulated by their model decreased when far away from the spinneret which was opposite to the real profile of fiber whipping according to the experimental recordings [9,13,22]. In addition, the amplitude of fiber obtained from their numerical model was smaller than the real profile by several magnitudes. That was the obviously disadvantage for their model. Later, Han *et al*. [23] used this Euler-Lagrange approach to simulate fiber path by applying differential mechanical fiber models (unlike Maxwell model used by Sun *et al*. [21]), the disadvantage appeared again.

In this study, the fiber whipping in melt blowing was simulated by an improved Lagrangian numerical approach. Here, this numerical approach was devoted to simulate the fiber whipping similarly to the real whipping profile, especially, refer to the lateral amplitude. The fiber whipping simulated in this study was compared with the real fiber paths obtained from experiments. Meanwhile, the fiber diameter, fiber velocity and fiber temperature as the distance below the spinneret were traced during the whole process of simulating iterations. This numerical simulation illustrated that it was

*Corresponding author: shengxie16@163.com

likely to exist an energy wasting of the fiber temperature and the relative velocity of fiber and air in melt blowing. At last, the optimizing design of air flow field for energy saving in melt blowing was discussed.

Experimental

Numerical Simulation

Our previous work [13] discovered that, in slot-die melt blowing, the fiber whipping path in the region near the spinneret was almost in 2-dimemsions. It was due to the dual converging air jets from the melt blowing device can be assumed to be 2-dimensional at positions below the spinneret [2,5,7,24]. In this numerical simulation, a 2-dimensional numerical simulation was applied for simulating the fiber whipping. As shown in Figure 1(a), the fiber whipping was assumed in *x*-*z* plane, the *x* direction is the lateral direction, and the *z* direction is directed vertically downward (along the spinning line).

Description of the Fiber Model

In this numerical simulation, the stream of polymer is defined as fiber, the polymeric fiber behaves the typical characteristic of viscoelasticity. In this part, the viscoelasticity is carried out by regarding the fiber into beads which connect with a Maxwell elements, each Maxwell element contains of a Newton's spring and a dashpot in series. The Newton's spring and dashpot represent the elasticity and viscosity of the polymeric fiber, respectively. As shows in Figure 1(b),

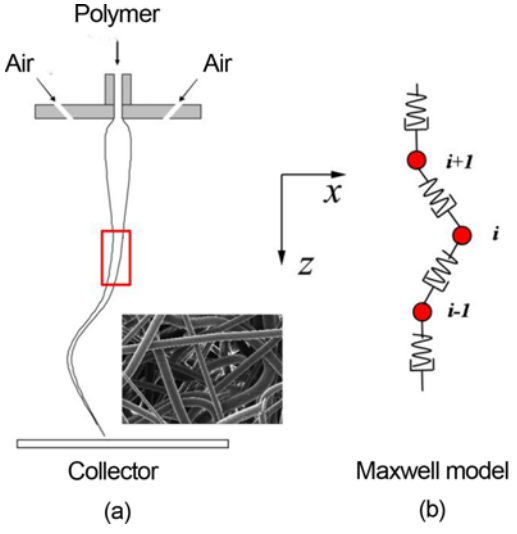

Figure 1. (a) The schematic of polymer attenuation by the air in slot-die melt blowing and (b) the Maxwell model for fiber in this numerical simulation. A Maxwell element contains of a Newton's spring and a dashpot in series. According to the previous work [13], the fiber whipping was assumed in *x*-*z* plane, the *x* direction is the lateral direction, and the *z* direction is directed vertically downward.

take bead *i* for an analytical unit, a pair of adjacent beads, *i*−1 and *i*+1, form the two fiber elements (*i*−1, *i* and *i*, *i*+1), the length of each element are given by

$$l_{i,i+1} = [(x_i - x_{i+1})^2 + (z_i - z_{i+1})^2]^{1/2} \quad (1\text{-}1)$$

$$l_{i-1,i} = [(x_i - x_{i-1})^2 + (z_i - z_{i-1})^2]^{1/2} \quad (1\text{-}2)$$

In this model, the mass of the bead *i*, m_i, is consisted by element (*i*−1, *i*) and element (*i* , *i*+1), and m_i is described as

$$m_i = \frac{1}{2}\rho_f A_{i-1,i} l_{i-1,i} + \frac{1}{2}\rho_f A_{i,i+1} l_{i,i+1} \quad (2)$$

where ρ_f and A represent the fiber density and the cross-sectional area of the fiber, respectively (During the simulating process, the mass of the bead *i* is keep constant, its diameter is dependence on the length of *l*. For example, during simulation, the new length of the bead is changed to be *l*, and *l* was bigger than the initial *l*, that means the fiber is stretched, and the fiber diameter can be calculated by the law of conservation of mass). And $A_{i\text{-}1,i}$ and $A_{i,i+1}$ are defined as

$$A_{i-1,i} = \frac{1}{4}\pi d_{i-1,i}^2 \quad (3\text{-}1)$$

$$A_{i,i+1} = \frac{1}{4}\pi d_{i,i+1}^2 \quad (3\text{-}2)$$

where $d_{i\text{-}1,i}$ and $d_{i,i+1}$ are the fiber average diameter of element (*i*−1, *i*) and (*i*, *i*+1), respectively. Here, it is noted that for the downmost bead, bead 1, the adjacent bead is only bead 2, so, m_1, is special and described as

$$m_1 = \frac{1}{2}\rho_f A_{1,2} l_{1,2} \quad (4)$$

Equations for Fiber Whipping

In melt blowing, the forces applied on beads (fiber) are air drag force from the air flow field, viscoelastic force contributed by the adjacent beads, gravity and fiber surface tension which is tend to keep the linear shape of the fiber. According to the conclusions of Sun *et al*. [21], compared to the air drag force and viscoelastic force, the surface tension is much smaller, in this numerical simulation, the surface tension is out of consideration.

Air Drag Force

The air drag force applied on the fiber elements can be decomposed into two components: friction drag and pressure drag. (1) Friction drag is contributed by the relative velocity of air and fiber which is parallel to the axis of fiber element, (2) pressure drag, which is contributed by the relative velocity normal to the axis of fiber element. Friction drag and pressure drag on bead *i*, F_{fi} and F_{pi}, are also contributed by the adjacent elements, they are described as

$$\mathbf{F}_{fi} = \frac{1}{2} C_f \rho_a v_{ref(i,i+1)} \pi d_{i,i+1} l_{i,i+1} \left[\frac{x_{i+1} - x_i}{l_{i+1,i}} \mathbf{i} + \frac{z_{i+1} - z_i}{l_{i+1,i}} \mathbf{k} \right] - \frac{1}{2} C_f \rho_a v_{ref(i-1,i)} \pi d_{i-1,i} l_{i-1,i} \left[\frac{x_{i+1} - x_i}{l_{i-1,i}} \mathbf{i} + \frac{z_{i+1} - z_i}{l_{i-1,i}} \mathbf{k} \right] \quad (5\text{-}1)$$

$$\mathbf{F}_{pi} = \frac{1}{2} C_n \rho_a v_{ren(i,i+1)} \pi d_{i,i+1} l_{i,i+1} \left[\frac{x_{i+1} - x_i}{l_{i+1,i}} \mathbf{i} + \frac{z_{i+1} - z_i}{l_{i+1,i}} \mathbf{k} \right] - \frac{1}{2} C_n \rho_a v_{ren(i-1,i)} \pi d_{i-1,i} l_{i-1,i} \left[\frac{x_{i+1} - x_i}{l_{i-1,i}} \mathbf{i} + \frac{z_{i+1} - z_i}{l_{i-1,i}} \mathbf{k} \right] \quad (5\text{-}2)$$

where C_f and C_N are the coefficient of friction drag and pressure drag, respectively; ρ_a is the air density; v_{ref} and v_{ren} are the relative velocity component parallel and normal to the axis of the fiber element, respectively; $\mathbf{r}_i = x_i\mathbf{i} + z_i\mathbf{k}$ is the position of bead i in the Cartesian coordinate system.

In equations (5-1) and (5-2), C_f and C_N are function of Reynolds number. Shambaugh and his coworkers devoted some works to determine the coefficients of C_f and C_N. Majumdar and Shambaugh [25] recommended C_f as

$$C_f = 0.78 \mathrm{Re}_f^{-0.61} \quad (6\text{-}1)$$

Ju and Shambaugh [26] determined C_N as

$$C_N = 6.96 \mathrm{Re}_n^{-0.440} \left(\frac{d}{7.8 \times 10^{-5}} \right)^{0.404} \quad (6\text{-}2)$$

Here, the Reynold Re_f and Re_N are given by

$$\mathrm{Re}_f = \frac{\rho_a v_{ref} d}{\mu_a} \quad (7\text{-}1)$$

$$\mathrm{Re}_N = \frac{\rho_a v_{reN} d}{\mu_a} \quad (7\text{-}2)$$

Viscoelastic Force

The fiber is regarded as a series of beads, the tensile stress acting along the fiber elements, (i–1, i), is described as

$$\frac{d\sigma_{i-1,i}}{dt} = \frac{E}{l_{i-1,i}} \frac{dl_{i-1,i}}{dt} - \frac{E\sigma_{i-1,i}}{\mu_f} \quad (8)$$

where, E is the elasticity modulus of fiber; μ_f is the viscosity of the fiber. Then, the viscoelastic force of bead i, $\boldsymbol{F}_{vei}$, contributed by the adjacent beads is given by

$$\mathbf{F}_{vei} = \sigma_{i,i+1} \frac{1}{4} \pi d_{i,i+1}^2 \left[\frac{x_{i+1} - x_i}{l_{i,i+1}} \mathbf{i} + \frac{z_{i+1} - z_i}{l_{i,i+1}} \mathbf{k} \right] - \sigma_{i-1,i} \frac{1}{4} \pi d_{i-1,i}^2 \left[\frac{x_{i+1} - x_i}{l_{i-1,i}} \mathbf{i} + \frac{z_{i+1} - z_i}{l_{i-1,i}} \mathbf{k} \right] \quad (9)$$

Equation (8) indicates that the tensile stress, σ, is partly depends on the fiber viscosity, μ_f. And μ_f has great relationship with fiber temperature. In this numerical simulation, the heat transfer relationship between the air and bead i is described as

$$m_i C_i \frac{dT}{dt} = -h\pi \left(\frac{d_{i-1,i} + d_{i,i+1}}{2} \right) \left(\frac{l_{i-1,i} + l_{i,i+1}}{2} \right) (T_i - T_{ai}) \quad (10)$$

where, C_i is the fiber heat capacity; T_i is the temperature of bead i; T_{ai} is the temperature of the air at position of bead i; h is the convective heat transfer coefficient.

In this numerical simulation, the initial temperature of the fiber is 385 °C.

The motion of the bead i can be calculated under the Newton's second law as the following formula

$$m_i \mathbf{a}_i = \frac{d^2 \mathbf{r}_i}{dt^2} = \mathbf{F}_{fi} + \mathbf{F}_{pi} + \mathbf{F}_{vei} + m_i \mathbf{g} \quad (11)$$

where, $\mathbf{a}_i$ is the accelerated speed of bead i; $\mathbf{F}_{fi}$, $\mathbf{F}_{pi}$, $\mathbf{F}_{vei}$ are described in equations (5) and (9); $m_i\mathbf{g}$ is the gravity of the bead i.

Air Flow Field Used in the Numerical Simulation

The air velocity and air temperature applied on the beads are cited from Uyttendaele and Shambaugh [14], they measured the air velocity and the air temperature in melt blowing with a fine, 0.45 mm-diameter pitot tube and a 0.51 mm-diameter thermocouple, respectively. In addition, these datas were matched in to mathematic formulas by them. It is noted that the profiles of air velocity and air temperature measured by them are representative, for their datas are similarly with other measurements [7,8,27-29].

Simulation Procedures

The time evolution of bead i in the numerical simulation is set by the following procedures:

(1) At time t=0, two beads, bead 1and bead 2, were existed below the spinneret. Here, the distance between the two beads was set to be 1×10^{-3} m and the average diameter of the element (1, 2) was set to be 5×10^{-4} m which was according to the diameter of the spinneret, the initial tensile stress between the two beads was set to be zero. At this time, the air velocity and air temperature were imported onto the two beads.

(2) The time step size for this numerical simulation was set to be 1×10^{-5} s, at the given time, 1×10^{-5} s, the new position of the two beads are calculated by equation (11) under the Newton's second law. Meanwhile, the air velocity and air temperature at the new position of the beads were imported onto the two beads. The air force, fiber density, fiber viscosity *et al*. are updated for the next step's calculation.

(3) The bead diameter was calculated by the law of conservation of mass. Because of the displacement of the two beads, the tensile stress starts to be generated. Until now, the resultant force can be calculated from air force, viscoelasitic

force and gravity.

(4) Repeated the iterative procedures (2) and (3). Due to the fiber in melt blowing was extruded out from the spinneret successively and steadily, in this numerical simulation, the successive stream of the beads was carried out by the method as follows: after an each given time, 0.01 s, a new bead was generated at the position of the initial bead 2 at t=0.

To simulate the fiber whipping, a 2-dimensional lateral disturb was applied on the new coming bead, the disturb equation was given by

$$x = \Delta x \cos(\omega t) = 1 \times 10^{-3} \cos(1000t) \quad (12)$$

(5) Because of the special position of the downmost bead, bead 1, in the simulating iteration process, when other bead, like bead 2, reached to the given position, the iteration terminated.

Parameter Verification

Actually, the simulation results are mainly dependent on the computation conditions. In this part, the effect of the length of the first two beads, the lateral disturb, Δx, the lateral disturb frequency, ω, and the time step size (which were mentioned in the section of simulation procedures) on the simulation results were discussed.

In this part, the simulated fiber path and simulated fiber diameter as criterions to judge the effect of these parameters onto the simulation. Here, for the criterion of simulated fiber path, if the simulated lateral amplitude increased when far away from the spinneret, the effect of parameters onto the model assumed to be acceptable. For the criterion of simulated fiber diameter, if the simulated fiber diameter decreased rapidly near the spinneret and then decreased gradually far away from the spinneret [30], the parameters applied in the simulation were also assumed to be acceptable.

Figure 2 to Figure 5 show the effect of these parameters onto the simulation results. For the fiber paths, the simulated lateral amplitude increased when far away from the spinneret, that illustrates the parameters used in this simulation are acceptable. It is noted that, as showed in Figure 5(a), the time step size has some effect onto the simulated fiber amplitude, the simulated fiber amplitude increased when the time step size increased from 10^{-6} s to 10^{-5} s, that means the

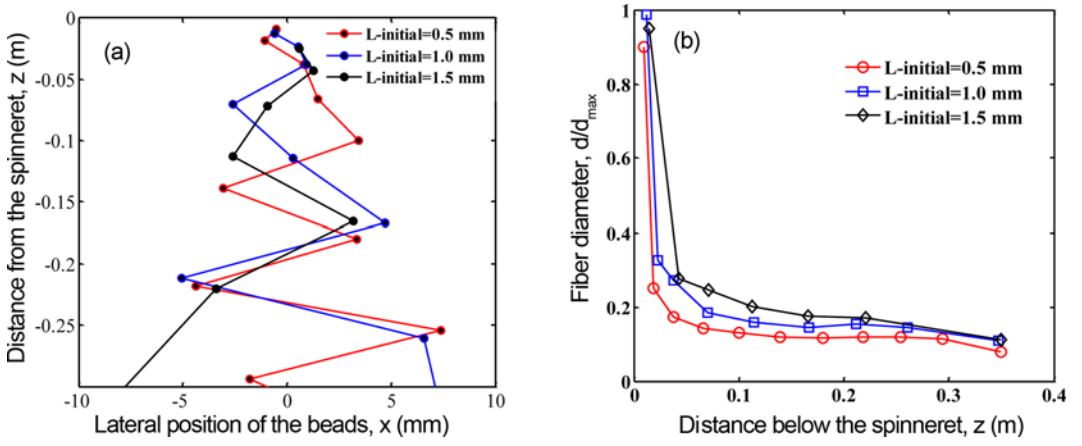

Figure 2. The effects of the length of the first initial two beads on (a) the simulated fiber paths and (b) the simulated fiber diameter.

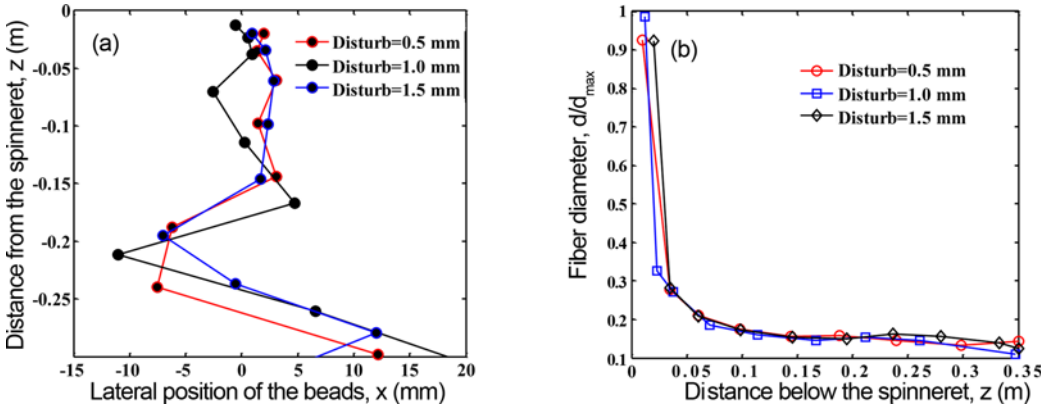

Figure 3. The effects of the lateral disturb, Δx, on (a) the simulated fiber paths and (b) the simulated fiber diameter.

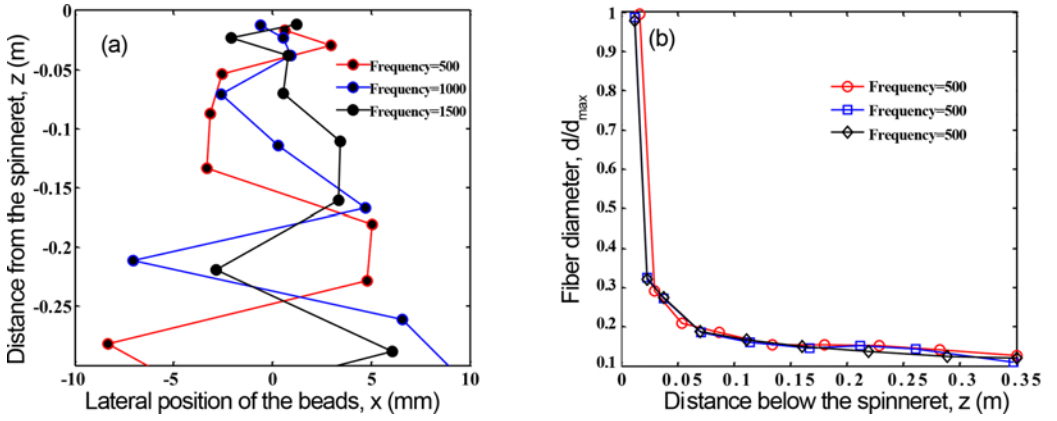

Figure 4. The effects of the lateral disturb frequency, ω, on (a) the simulated fiber paths and (b) the simulated fiber diameter.

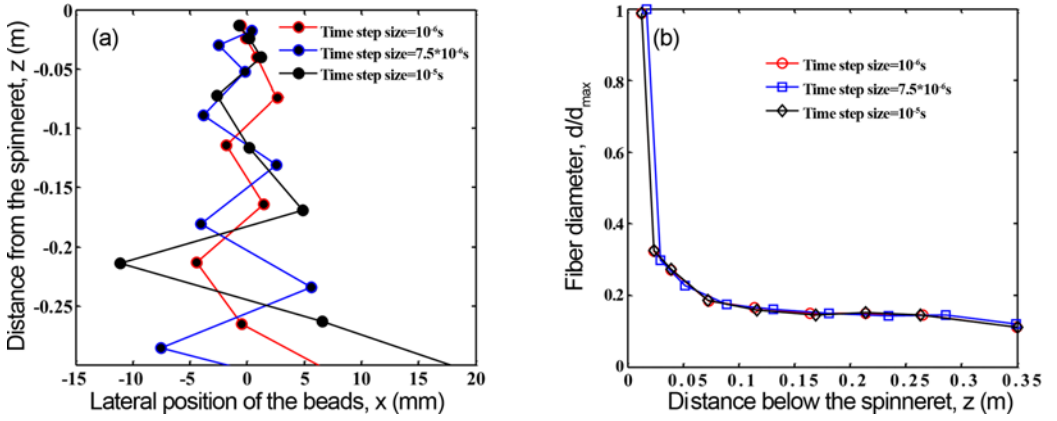

Figure 5. The effects of the time step size on (a) the simulated fiber paths and (b) the simulated fiber diameter.

fiber whipping motion can be demonstrated sufficiently when the time step size was set to 10^{-5} s. For the simulated fiber diameter, all the parameters used in this part result in acceptable tendency of fiber decreasing profile, for Figures 2-5(b) show the fiber diameter decreased rapidly in the region less than 5 mm below the spinneret, then the fiber diameter decreased gradually.

Results and Discussion

Figure 6 compares the fiber whipping path obtained by this numerical simulation and by experimental method. Figure 6(a) shows that the fiber whipping generated alternately around the *z*-axis after it comes out from the spinneret. An obviously characteristics of the fiber whipping is the lateral (*x*-direction) amplitude increases gradually when fiber moves away from the spinneret. Figure 6(b) is the fiber path obtained by experiments in our previous work [13], the fiber path in the slot-die melt blowing was captured by a high-speed camera at a frame rate of 5000 frames/s, and the real image size of the image is 26.2 mm×19.6 mm. The experimental result indicated that fiber whipping in the slot-die melt blowing appears to be a fiber path with two groups of loops moving downward. The outline of the fiber path presented a cone envelope. Figure 6 illustrates that the fiber whipping simulated in this part is basically accordant with the real path in melt-blowing process.

Figure 7 compares the lateral amplitude of fiber whipping obtained by this numerical simulation and experiment, the cone envelope is used to reflect the lateral amplitude. Figure 7(a) shows the cone envelope of the simulated fibers which are constituted by 5 fiber whipping paths overlapped. The coordinated position of the most lateral beads (z, x) are fitted mathematically by liner regress equations, the liner regress equations represents the cone envelope of the fiber, signed as the dotted line in Figure 7(a), which is

$$x = 49.822z \ (R^2 = 0.73) \tag{13}$$

Figure 7(b) shows the bundle of fibers obtained by Shambaugh and his coworkers [9] via high speed camera, the splaying fiber paths are constituted with some successive flashes spaced at intervals of 0.01 s. The mathematic equation of cone envelope is regressed to the mathematic formulas

$$x = 56.667z \tag{14}$$

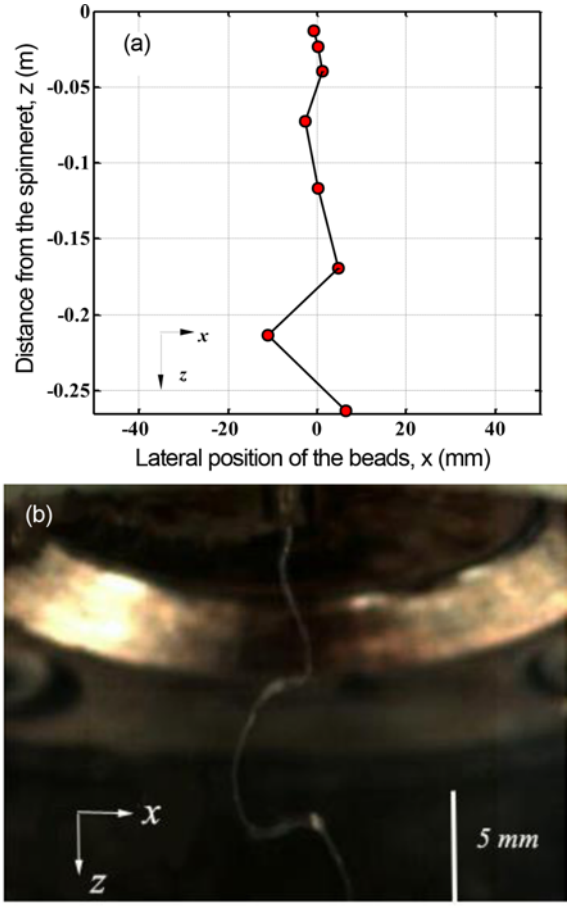

Figure 6. (a) The fiber whipping path simulated by the numerical approach. When bead 2 reached at about z=0.3 m, the iteration process terminated and (b) is the fiber path in slot-die melt blowing obtained by high-speed camera at a frame rate of 5000 frames/s, the real image size of the image is 26.2 mm×19.6 mm.

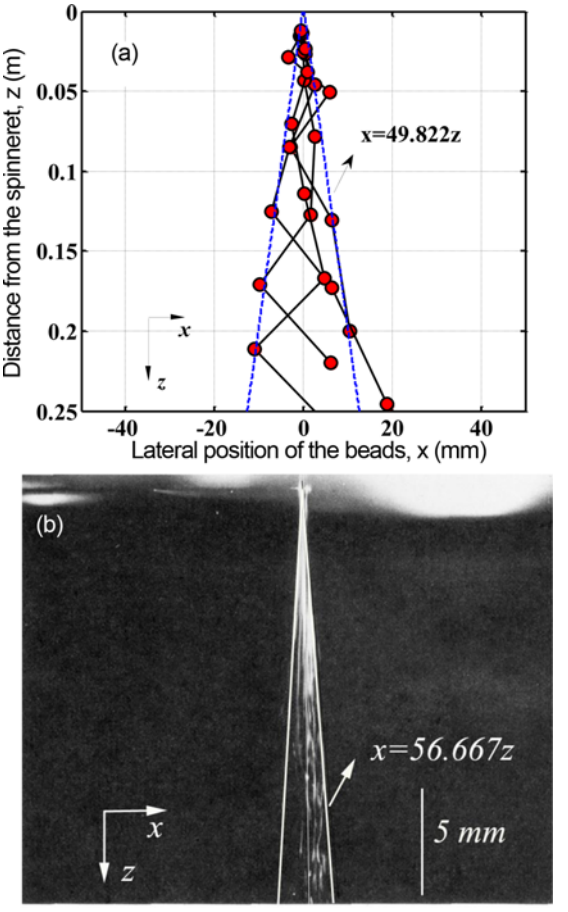

Figure 7. (a) The cone envelope of the simulated fibers which are constituted by 5 fiber whipping paths overlapped and (b) The bundle of fibers obtained by Shambaugh and his coworkers [9] via high speed photograph, the high-speed photograph of the melt blowing process was captured from 0 to 20 mm below the spinneret.

The monomial coefficients of the regressed formulas are 49.882 and 56.667 for the simulation and experiments, respectively. That shows the numerical simulating model for predicting the fiber whipping especially in lateral direction is closed to the actual. The difference of these monomial coefficients may be on account of some parameters used in this numerical simulation is inconsistent with the real in their experiments.

Figure 8 indicates the simulated fiber diameter as the distance below the spinneret, z, as well as the fiber diameter measured by Shambaugh and his coworkers [27]. The maximum of the fiber diameter, d_{max}, is regarded as the diameter of the spinneret. As the simulation shows in Figure 8, the fiber diameter decreases rapidly to 20 % of d_{max} in a short region below the spinneret within about 0.07 m, later, the fiber diameter decreases gradually. This simulating conclusion also illustrates that the researching on the air flow field and the fiber motion near the spinneret is crucial. The fiber diameter measured by Shambaugh and his

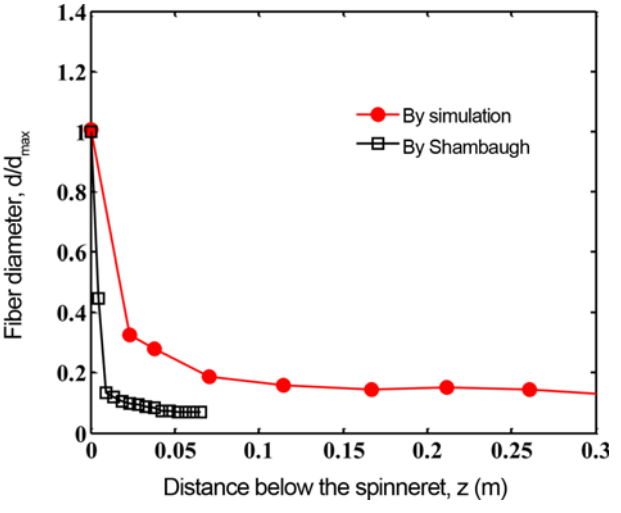

Figure 8. The numerical simulated fiber diameters as well as the fiber diameters measured by Shambaugh and his coworkers [30].

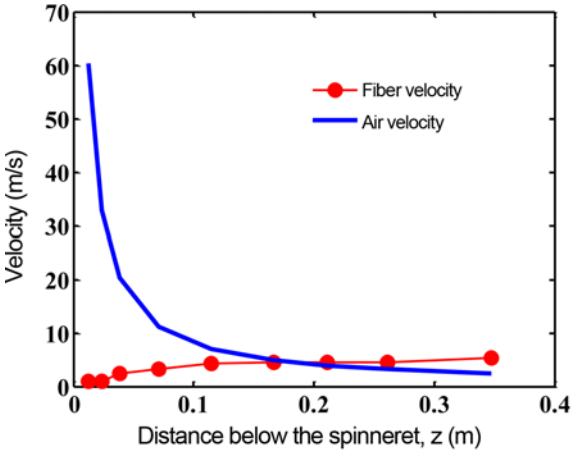

Figure 9. The air velocity as well as the numerical simulated fiber velocity as the distance below the spinneret, z. Both velocities become equal at a critical z-position, z=0.18 m.

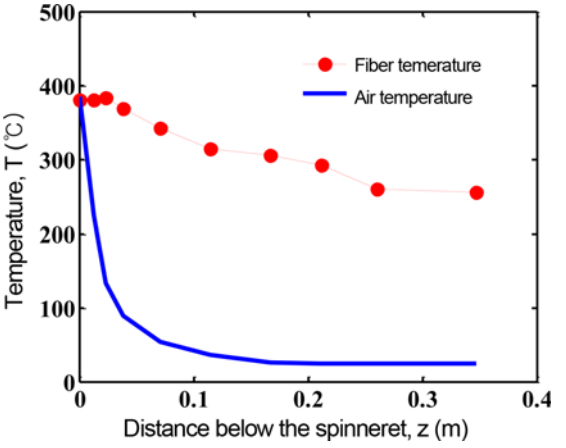

Figure 10. The temperature of the fiber and the air as the distance below the spinneret, z.

coworkers [30] also shows the region where the most decreasing of fiber diameter is about 0.03 m below the spinneret. The fiber diameter simulated by this numerical approach is larger than the experimental measurements, that is dominantly due to the polymer flow rate and the air velocity are obviously different between this numerical simulation and their experiments.

Figure 9 shows the relationship between the air velocity and the simulated fiber velocity as the distance below the spinneret, z, in melt blowing. The air velocity is cited from Uyttendaele and Shambaugh [14]. In melt blowing process, the air velocity decreases along the spinning line (z-axis), the air velocity is about 60 m/s at z=0.012 m, and it decreases to be less than 10 m/s when $z \geq 0.07$ m. While, the fiber velocity increases gradually when downward moves to the collector. It is noted that the fiber velocity will increase to be equal with the air velocity at a critical z-position (in this numerical simulation, z=0.18 m), and the fiber velocity becomes larger than the air velocity where below the critical z-position. This phenomenon illustrates that when the fiber below the critical z-position, the air velocity doesn't apply the attenuating effect on the fiber, inversely, results in the fiber's rebound.

Figure 10 shows the temperature of the fiber and the air according to the distance below the spinneret, z. Similar with the profile of the air velocity in Figure 9, the air temperature decreases rapidly near the spinneret. At z=0, according to Uyttendaele and Shambaugh [14], the initial air temperature is 385 °C and decreases to be less than 35 °C in the region where $z \geq 0.11$ m. Unlike the rapidly decreasing of air temperature, the fiber temperature decreases gradually when moves far away from the spinneret. The heat of the air transfers to the fiber immediately, however, the heat of the fiber transfers to the adjacent air tardily even if the air temperature is much lower than the fiber temperature. It is due to that the fiber is surrounded by the hot air, while the hot air is surrounded by the adjacent air with normal temperature in larger exchange area.

From Figures 9 and 10, such as at the position of z=0.3 m, the fiber temperature is still high, for the mostly common-used material in melt blowing, polypropylene (PP), its melting point is about 165 °C, it indicates that the fiber is still under the status of molten, and the fiber can be attenuated easily by the air with higher velocity. However, as Figure 9 shows, at z=0.3 m, the air velocity decreases to be lower than the fiber velocity, the molten fiber rebound inevitably. In another description, in this example, there is an energy wasting in the melt blowing process, for the temperature of the fiber is higher than its melting point while the air attenuating effect disappears. It is also indicates that the optimizing design of the melt-blowing air field is very crucial for fiber attenuation and energy saving. We suppose that the optimized air flow field deserves to contain these characteristics: when the air velocity is larger than the fiber velocity, the fiber is keep molten, or when the air velocity is lower than the fiber velocity, the fiber changes to be solidified and vice versa.

Conclusion

In this study, an improved numerical simulating model was built to simulate the fiber whipping in melt-blowing process, the path of the fiber, the lateral position of the fiber, and the fiber diameter, fiber velocity, fiber temperature as the distance below the spinneret were predicted.

This improved numerical approach overcame the disadvantage existed in the previous works used Lagrangian model. This improved approach simulated the fiber whipping which was similar to the real path captured by experiments especially referred to the lateral position of the fiber. These simulations predicted that the fiber velocity increases gradually, while, the air velocity decreases rapidly as the

distance below the spinneret. There was a critical *z*-position where both velocities became to be equal; these simulations also predicted that the fiber temperature keeps high compared to the air temperature. This numerical simulation illustrated that the fiber temperature and the relative velocity of fiber and air should be utilized optimally for energy saving in melt blowing, this work may provide a referential ideas for energy saving problems in melt blowing.

Acknowledgement

This research was supported by the National Natural Science Foundation of China (Grant 11272088 and Grant 51506075), Chinese Universities Scientific Fund (Grant 13D310117 and Grant 101-06-0019044).

References

1. H. M. Krutka, R. L. Shambaugh, and D. V. Papavassiliou, *Ind. Eng. Chem. Res*., **41**, 5125 (2002).
2. H. M. Krutka, R. L. Shambaugh, and D. V. Papavassiliou, *Ind. Eng. Chem. Res*., **43**, 4199 (2004).
3. E. M. Moore, R. L. Shambaugh, and D. V. Papavassiliou, *J. Appl. Polym. Sci*., **94**, 909 (2004).
4. H. M. Krutka, R. L. Shambaugh, and D. V. Papavassiliou, *Ind. Eng. Chem. Res*., **45**, 5098 (2006).
5. A. S. Harpham and R. L. Shambaugh, *Ind. Eng. Chem. Res*., **35**, 3776 (1996).
6. B. D. Tate and R. L. Shambaugh, *Ind. Eng. Chem. Res*., **37**, 3772 (1998).
7. A. S. Harpham and R. L. Shambaugh, *Ind. Eng. Chem. Res*., **36**, 3937 (1997).
8. B. D. Tate and R. L. Shambaugh, *Ind. Eng. Chem. Res*., **43**, 5405 (2004).
9. R. S. Rao and R. L. Shambaugh, *Ind. Eng. Chem. Res.*, **32**, 3100 (1993).
10. R. R. Bresee and W. C. Ko, *Int. Nonwovens J.*, **12**, 21 (2003).
11. R. R. Bresee, *Int. Nonwovens J.*, **11**, 27 (2002).
12. R. R. Bresee, *Int. Nonwovens J.*, **11**, 21 (2002).
13. S. Xie and Y. C. Zeng, *Ind. Eng. Chem. Res.*, **52**, 2116 (2013).
14. M. A. Uyttendaele and R. L. Shambaugh, *AICHE J.*, **36**, 175 (1990).
15. V. T. Marla and R. L. Shamaugh, *Ind. Eng. Chem. Res.*, **42**, 6993 (2003).
16. T. Chen and X. B. Huang, *Text. Res. J*., **73**, 651 (2003).
17. D. H. Tan, C. F. Zhou, C. J. Ellison, S. Kumar, C. W. Macosko, and F. S. Bates, *J. Non-Newton. Fluid Mech*., **165**, 892 (2010).
18. C. Chung and S. Kumar, *J. Non-Newton. Fluid Mech*., **192**, 37 (2013).
19. C. Zhou, D. H. Tan, A. P. Janakiraman, and S. Kumar, *Chem. Eng. Sci.*, **66**, 4172 (2011).
20. D. H. Tan, P. K. Herman, A. Janakiraman, F. S. Bates, S. Kumar, and C. W. Macosko, *Chem. Eng. Sci.*, **80**, 342 (2012).
21. Y. F. Sun, Y. C. Zeng, and X. H. Wang, *Ind. Eng. Chem. Res.*, **50**, 1099 (2011).
22. H. Jessica, R. L. Shambauhg, B. R. Shambaugh, and D. W. Schmidtke, *Ind. Eng. Chem. Res.*, **46**, 7340 (2007).
23. W. L. Han and X. H. Wang, *Fiber. Polym.*, **17**, 74 (2016).
24. H. M. Krutka, R. L. Shambaugh, and D. V. Papavassiliou, *Ind. Eng. Chem. Res*., **42**, 5541 (2003).
25. B. M. Majumdar and R. L. Shambaugh, *J. Rheol*., **34**, 591 (1990).
26. Y. D. Ju and R. L. Shambaugh, *Polym. Eng. Sci*., **34**, 958 (1994).
27. T. Chen, X. H. Wang, and X. B. Huang, *Text. Res. J*., **74**, 1018 (2004).
28. Y. E. Lee and L. C. Wadsworth, *J. Appl. Polym. Sci*., **105**, 3723 (2007).
29. Y. F. Sun, B. W. Liu, and X. H. Wang, *J. Appl. Polym. Sci*., **122**, 3520 (2011).
30. B. Vishal and R. L. Shambaugh, *Ind. Eng. Chem. Res*., **37**, 1799 (1998).